Preprints of the 21st IFAC World Congress (Virtual)
Berlin, Germany, July 12-17, 2020

Wave Excitation Force Estimator Using Kalman Filtering Approach for Point Absorber Wave Energy Converters Under Different Modeling and Operation Scenarios

Mohammed A. Jama * **Addy Wahyudie.** **

* *Emirates Centre of Energy and Environment Research (ECEER), UAE University, Al Ain, UAE (e-mail: m.jama@uaeu.ac.ae).*
** *Electrical Engineering Department, UAE University, Al Ain, UAE (e-mail: addy.w@uaeu.ac.ae)*

Abstract: In this research, one of the most important research questions that influence the effectiveness of the used control strategies in heaving wave energy converters (WECs) is addressed. A nonlinear extended Kalman filter (EKF) based state estimator to estimate the wave excitation force and heave velocity in real-time is proposed. A holistic nonlinear model involving both the mechanical and electrical sides of the WEC system is used. The proposed estimator was compared with a simpler linear Kalman filter (KF) estimator under varying sea state environment and electric loading conditions. Generally, both estimators produced "statistically" good estimates, however, the EKF estimators outperformed its counterpart in both the estimation accuracy and maintaining low incident energy drop.

Keywords: Wave energy, wave energy converter, state estimation, extended Kalman filter, excitation force.

1. INTRODUCTION

The wave excitation force is a hydrodynamic force that is applied by the incoming waves on the buoy when it is held motionless (i.e., its velocity is zero). Despite being the main driving force of the system, the wave excitation force usually poses challenges to the engineers involved in designing and developing wave energy technologies. Accurate knowledge of the wave excitation force applied on the WEC buoy is crucial in the design (pre-deployment) stage and also during operation. In the design stage, accurately calculating the wave excitation force is important to properly design the buoy geometry and size the corresponding PTO system. While accurate real-time knowledge of the excitation force – through measurement or estimation – is important for implementing effective control strategies that ensure optimum power absorption, system reliability, and durability. To implement real-time control strategies to control WECs, the wave excitation force needs to be calculated or measured at every time instant (Babarit and Clement (2006)). As for the excitation force calculation, a linear causal relationship between the wave elevation and the wave excitation force is approximated by solving the excitation force problem for various wave frequencies using hydrodynamic numerical tools such as WAMIT (Taghipoura et al. (2008)). Note that this method assumes the wave propagation in space and time as a linear system (i.e., linear wave theory) and it also causalizes the originally non-causal relation between the wave excitation force and the incoming wave elevation. Therefore, any real-time calculation of the excitation force using the wave elevation time series is only an approximation of what is actually experienced by the buoy. One more issue in this method is the need to carry out wave elevation measurement upstream of the location of the WEC that is the wave elevation measurement is not available in the vicinity of the WEC which makes this method even more complex to be implemented in real-time. Another method to obtain the excitation force values in real-time is to measure the hydrodynamic pressure applied at the wetted surface area of the buoy (Falnes (2002)).

A simple linear Luenberger observer used to instantaneously estimate the excitation torque is presented in (Kracht et al. (2015)). The linear observer was part of an overall servo-tracking control problem where the buoy velocity is manipulated to track a pre-determined reference velocity using the estimated excitation force. Although the control strategy was tested experimentally, a simplified WEC model was used to construct the observer – that is no nonlinearities were involved. In (Abdelkhalik et al. (2016)), an extended Kalman filter is used to estimate the wave excitation force using measurements of the hydrodynamic pressure at various points of the buoy wetted surface and the buoy position. No control force is applied – that is buoy was freely oscillating. The reported estimator requires large number of pressure transducers which will

⋆ This work was supported in part by the Joint Research Program between UAE University and Asian Universities Alliance (AUA) under Grant 31R169.
**Corresponding author: addy.w@uaeu.ac.ae

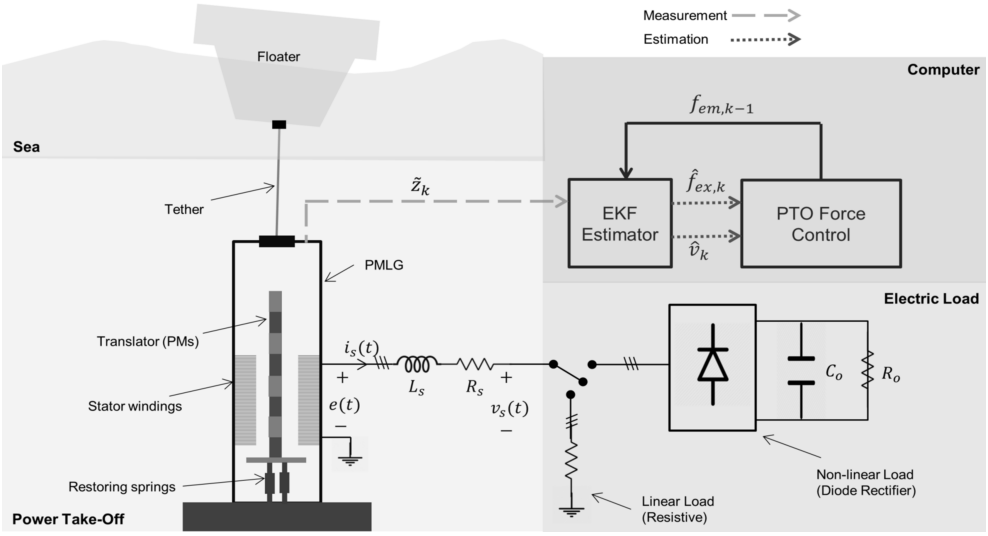

Fig. 1. Schematic of the investigated WEC system along with the estimator.

further exacerbate the computational complexity of the estimator. A simple linear Kalman filter estimator coupled with a random walk model is discussed in (Nguyen and Tona (2017)). The Kalman filter is based on a linear WEC model, where the buoy motion states (i.e., position and velocity) along with PTO control force measurement via a load cell is fed to the estimator. The estimator goodness is verified experimentally.

In this work, a nonlinear state estimator based on extended Kalman filtering approach to estimate the heave wave excitation force and the floater heave velocity is proposed. A comprehensive nonlinear model of the WEC is deployed. The proposed estimator requires only two the real-time knowledge of two variables at a given time, that is, the floater heave displacement and the electromagnetic force applied by the power take-off (PTO) system. The highly nonlinear friction force that might result from the movement of the system parts against each other, was modeled using a differentiable version of the well-known Coulomb friction model with Stribeck and viscous effects. The wave excitation force is modeled as a random walk process with a drift. The goodness of the proposed estimator has been assessed in simulation as part of a complete wave-to-wire WEC system.

2. POINT ABSORBER WEC MODEL

In this study, a direct drive based semi-submerged point absorber wave energy converter (WEC) is investigated as shown in Fig. 1. The forces acting on the point absorber oscillating body in the heave degree-of-freedom of motion can be expressed using Newton's second law of motion (Jama et al. (2018)), as

$$f_h(t) + f_{pto}(t) = ma(t), \tag{1}$$

where $f_h(t)$, $f_{pto}(t)$ and $a(t)$ are the hydrodynamic, power take-off (PTO) forces and the heave acceleration of the oscillating body, respectively. m represents the total mass of the floater, the PMLG translator and the interconnecting tether. The hydrodynamic force is composed of the following forces,

$$f_h(t) = f_{ex}(t) + f_r(t) + f_b(t) + f_d(t) + f_f(t), \tag{2}$$

where $f_{ex}(t)$, $f_r(t)$, $f_b(t)$, $f_d(t)$, and $f_f(t)$ are the wave excitation, radiation, buoyancy, drag, and friction forces, respectively. The wave excitation force is modeled as the convolution of the excitation kernel function $k_{ex}(t)$ and the wave surface elevation $\eta(t)$,

$$f_{ex}(t) = k_{ex}(t) * \eta(t) = \int_0^t k_{ex}(\tau)\eta(t-\tau)d\tau \approx \boldsymbol{C}_e\boldsymbol{q}_e(t), \tag{3}$$
$$\dot{\boldsymbol{q}}_e(t) = \boldsymbol{A}_e\boldsymbol{q}_e(t) + \boldsymbol{B}_e\eta(t).$$

The wave excitation force can be approximated by a linear time-invariant (LTI) model characterized by the auxiliary state vector $\boldsymbol{q}_e(t)$ and the state matrices $\boldsymbol{A}_e$, $\boldsymbol{B}_e$ and $\boldsymbol{C}_e$. Similarly, the radiation force is modeled as,

$$f_r(t) = -m_\infty a(t) - \int_0^t k_r(\tau)v(t-\tau)d\tau. \tag{4}$$

Here, m_∞ and $k_r(t)$ are the added mass due to the water-floater interaction and the radiation kernel function, respectively. The radiation integral is approximated by

$$\int_0^t k_r(\tau)v(t-\tau)d\tau \approx \boldsymbol{C}_r\boldsymbol{q}_r(t), \tag{5}$$
$$\dot{\boldsymbol{q}}_r(t) = \boldsymbol{A}_r\boldsymbol{q}_r(t) + \boldsymbol{B}_r v(t),$$

where $\boldsymbol{q}_r(t)$ is the radiation auxiliary state vector and $\boldsymbol{A}_r$, $\boldsymbol{B}_r$ and $\boldsymbol{C}_r$ are the radiation force state matrices. The buoyancy force $f_b(t)$ is modeled as a function of heave displacement, where the buoyancy stiffness coefficient S_b is the constant of proportionality,

$$f_b(t) = -S_b z(t), \tag{6}$$

According to Morison's equation, the viscous drag force $f_d(t)$ of a floating body is modeled as a quadratic function of the relative velocity between the floater and the water surface (Kracht et al. (2013)),

$$f_d(t) = -0.5\rho A_w C_d |v(t) - v_f(t)|\big(v(t) - v_f(t)\big). \tag{7}$$

where ρ, A_w, C_d, and $v_f(t)$ are the water density, floater submerged surface area, drag coefficient and the water surface vertical velocity, respectively. The friction force between the moving parts of the WEC can be modeled using the well known Coulomb friction model with Stribeck and viscous effects, that is

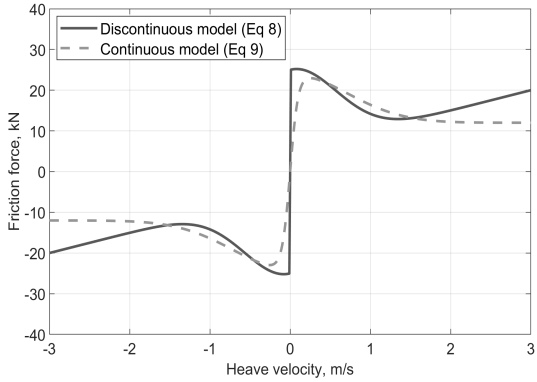

Fig. 2. Continuous friction model approximation compared to the discontinuous model

$$f_f(t) = -F_n\mu_d \operatorname{sign}\big(v(t)\big) - \mu_v v(t) - (\mu_s - \mu_d)e^{-(\frac{|v(t)|}{v_s})^2} \operatorname{sign}\big(v(t)\big), \tag{8}$$

where F_n, μ_d, μ_v, μ_s, and v_s are the normal force, the dynamic coefficient of friction, the viscous coefficient of friction, the static coefficient of friction and the Stribeck velocity, respectively. The friction force model in (8) is non-differentiable due to the discontinuity present in the Coulomb friction component (i.e., at $v(t) = 0$). Therefore, a continuous and differentiable approximation of the Coulomb's friction force model is needed. In (Brown and McPhee (2016)), a continuous velocity dependent friction model is proposed, as follows

$$f_f(t) \approx -F_n\mu_d \tanh\big(\alpha v(t)\big) - \mu_v v(t) - F_n(\mu_s - \mu_d)e^{-(\frac{|v(t)|}{v_s})^2} \tanh\big(\alpha v(t)\big). \tag{9}$$

The tunning parameter α determines the rate of increase of the friction force from zero to the static friction. The friction force models in (8) and (9) as function of heave velocity are shown in Fig. 2. The force exerted by power take-off (PTO) system is made of the summation of a spring restoring force $f_{rs}(t)$ and the PMLG electromagnetic force $f_{em}(t)$,

$$f_{pto}(t) = f_{rs}(t) + f_{em}(t), \tag{10}$$

where $f_{rs}(t) = -S_{rs}z(t)$, in which, S_{rs} is the PTO restoring spring coefficient. For PMLG, the linear electromagnetic force is directly proportional to the stator quadrature current. In this work, the PMLG is loaded with a three phase resistive load and a three phase diode rectifier, both providing a passive (damping) control action as shown in Fig. 1 (Jama and Wahyudie (2017)). The overall continuous nonlinear model of the system in state space form can be written as

$$\begin{aligned}
\dot{x}_1(t) &= x_2(t) \\
\dot{x}_2(t) &= \frac{1}{m+m_\infty}\Big[f_{ex}(t) - \boldsymbol{C}_r\boldsymbol{x}_3(t) - (S_b+S_{rs})x_1(t) \\
&\quad - 0.5\rho A_w C_d|x_2(t) - v_f(t)|\big(x_2(t) - v_f(t)\big) \\
&\quad - F_n\mu_d \operatorname{sign}\big(x_2(t)\big) - \mu_v x_2(t) \\
&\quad - (\mu_s - \mu_d)e^{-(\frac{|x_2(t)|}{v_s})^2} \operatorname{sign}\big(x_2(t)\big) + u(t)\Big], \\
\dot{\boldsymbol{x}}_3(t) &= \boldsymbol{A}_r\boldsymbol{x}_3(t) + \boldsymbol{B}_r x_2(t), \\
\boldsymbol{y}(t) &= [x_1(t), x_2(t)].
\end{aligned} \tag{11}$$

where the state vector $\boldsymbol{x}(t) = [x_1(t), x_2(t), \boldsymbol{x}_3(t)] = [z(t), v(t), \boldsymbol{q}_r(t)]$, the system input $u(t) = f_{em}(t)$ and the output vector $\boldsymbol{y}(t) = [x_1(t), x_2(t)]$. The wave radiation effect is modeled using 4th order linear model $\boldsymbol{q}_r(t) \in \mathbb{R}^{4\times1}$, therefore, the state vector $\boldsymbol{x}(t) \in \mathbb{R}^{6\times1}$

3. DERIVATION OF KALMAN FILTERING BASED ESTIMATORS

In this section, two state estimators are derived. The first being the linear Kalman filter based wave excitation force estimator, while the second is based on an extended Kalman filtering technique, allowing it to accommodate the nonlinear forces. Both estimators are designed to estimate the floater heave velocity alongside the wave excitation force. Practically, the estimators are fed with two measured signals, one being the floater heave displacement $z(t)$ using a position sensor and the other is the PTO electromagnetic force $f_{em}(t)$ using a force transducer (e.g., load cell). A schematic of the developed state estimators is shown in Fig. 3.

3.1 Discretization of the WEC Model

The first step to design the state estimators is to discretize WEC model. The system can be represented by the generic discrete nonlinear model as follows

$$\begin{aligned}
\boldsymbol{x}_k &= \boldsymbol{f}_{k-1}(\boldsymbol{x}_{k-1}, \boldsymbol{u}_{k-1}, \boldsymbol{w}_{k-1}), \\
\boldsymbol{y}_k &= \boldsymbol{g}_k(\boldsymbol{x}_k, \boldsymbol{\sigma}_k), \\
\boldsymbol{w}_k &\sim (\boldsymbol{0}, \boldsymbol{Q}_k), \boldsymbol{\sigma}_k \sim (\boldsymbol{0}, \boldsymbol{R}_k).
\end{aligned} \tag{12}$$

The functions $\boldsymbol{f}_{k-1}$ and $\boldsymbol{g}_k$ are nonlinear state and measurement functions at time instants $k-1$ and k, respectively. The state function estimates the system states at k using the state vector $\boldsymbol{x}_{k-1}$, the input vector $\boldsymbol{u}_{k-1}$, and the process noise vector $\boldsymbol{w}_{k-1}$ all evaluated at $k-1$. The process noise vector $\boldsymbol{w}_k$ and the measurement noise vector $\boldsymbol{\sigma}_k$ are modeled as a white noise with zero mean and known covariance matrices of $\boldsymbol{Q}_k$ and $\boldsymbol{R}_k$, respectively. Since the wave excitation force is meant to be estimated using other measured variables, the excitation force $f_{ex}(t)$ at time instant k is modeled as a simple random walk with drift process (Nguyen and Tona (2017)), that is

$$f_{ex,k} = f_{ex,k-1} + T_s\epsilon_{k-1}. \tag{13}$$

where T_s is the process sampling time and ϵ is the random walk drift modeled as a Gaussian noise with zero mean. Therefore, by updating the state vector in (11) to include $f_{ex,k}$, the modified state vector at k is represented as $\boldsymbol{x}_k = [x_{1,k}, x_{2,k}, \boldsymbol{x}_{3,k}, x_{4,k}] = [x_{1,k}, x_{2,k}, \boldsymbol{x}_{3,k}, x_{4,k}] = [z_k, v_k, \boldsymbol{q}_{r,k}, f_{ex,k}] \in \mathbb{R}^{7\times1}$. The process noise vector $\boldsymbol{w}_k = [w_{1,k}, w_{2,k}, \boldsymbol{w}_{3,k}, w_{4,k}] \in \mathbb{R}^{7\times1}$. Using the backward Euler method, the set of differential equations in (11) is transformed to difference equations, as follows

$$\begin{aligned}
x_{1,k} &= x_{1,k-1} + T_s\big[x_{2,k-1} + w_{1,k-1}\big], \\
x_{2,k} &= x_{2,k-1} + \frac{T_s}{m+m_\infty}\big[x_{4,k-1} - \boldsymbol{C}_r\boldsymbol{x}_{3,k-1} \\
&\quad - (S_b+S_{rs})x_{1,k-1} \\
&\quad - 0.5\rho A_w C_d(x_{2,k-1} - v_f)|x_{2,k-1} - v_f| \\
&\quad - F_n\mu_d \tanh\big(\alpha x_{2,k-1}\big) \\
&\quad - F_n(\mu_s - \mu_d)e^{-(\frac{|x_{2,k-1}|}{v_s})^2} \tanh\big(\alpha x_{2,k-1}\big) \\
&\quad - \mu_v x_{2,k-1} + u_{k-1}\big] + T_s w_{2,k-1}, \\
\boldsymbol{x}_{3,k} &= \boldsymbol{x}_{3,k-1} + T_s\big[\boldsymbol{A}_r\boldsymbol{x}_{3,k-1} + \boldsymbol{B}_r x_{2,k-1} \\
&\quad + \boldsymbol{w}_{3,k-1}\big],
\end{aligned} \tag{14}$$

$$x_{4,k} = x_{4,k-1} + T_s w_{4,k-1},$$
$$y_k = x_{1,k} + \sigma_k.$$

Note that the excitation force random walk drift ϵ_k in (13) is replaced with the system noise variable $w_{4,k-1}$ in (14).Moreover, the discretized version of the continuous friction model depicted in (8) is used instead of (7).

3.2 Linear Kalman Filter (KF) Estimator

The linear Kalman filter estimator is derived by linearizing the system model in (14). By omitting the drag force and friction force dynamics, the resultant linear model is

$$\boldsymbol{x}_k = \boldsymbol{A}_l \boldsymbol{x}_{k-1} + \boldsymbol{B}_l u_{k-1} + \boldsymbol{w}_{k-1}, \quad (15)$$
$$y_k = \boldsymbol{C}_l \boldsymbol{l}_k + \sigma_k,$$

where

$$\boldsymbol{A}_l = \begin{pmatrix} \boldsymbol{A}_d & \boldsymbol{B}_d \\ \boldsymbol{0}_{1\times 6} & 1 \end{pmatrix}, \boldsymbol{B}_l = \begin{pmatrix} \boldsymbol{B}_d \\ 0 \end{pmatrix}, \boldsymbol{C}_l = (\boldsymbol{C}_d \ 0)$$

The state matrices $\boldsymbol{A}_d$, $\boldsymbol{B}_d$, and $\boldsymbol{C}_d$ are the discrete counterparts of the following continuous state matrices

$$\boldsymbol{A} = \begin{pmatrix} 0 & 1 & \boldsymbol{0}_{1\times 4} \\ -\dfrac{S_b + S_{rs}}{m + m_\infty} & 0 & -\dfrac{\boldsymbol{C}_r}{m + m_\infty} \\ \boldsymbol{0}_{4\times 1} & \boldsymbol{B}_r & \boldsymbol{A}_r \end{pmatrix}, \boldsymbol{B} = \begin{pmatrix} 0 \\ \dfrac{1}{m + m_\infty} \\ \boldsymbol{0}_{4\times 1} \end{pmatrix},$$
$$\boldsymbol{C} = (1\ 0\ 0\ 0\ 0\ 0).$$

Initializing the posteriori estimate of the state vector as $\hat{\boldsymbol{x}}_o^+ = \boldsymbol{0}_{1\times 7}$ and the posteriori estimation error covariance matrix as $\boldsymbol{P}_o^+ = \boldsymbol{0}_{7\times 7}$, the state estimate $(\hat{x}_k^+)$ is computed at every sampling instant using the following equations

$$\boldsymbol{P}_k^- = \boldsymbol{A}_l \boldsymbol{P}_{k-1}^+ \boldsymbol{A}_l^\top + \boldsymbol{Q}_{kf,k-1}, \quad (16)$$
$$\boldsymbol{K}_k = \boldsymbol{P}_k^- \boldsymbol{C}_l^\top (\boldsymbol{C}_l \boldsymbol{P}_k^- \boldsymbol{C}_l^\top + \boldsymbol{R}_{kf,k})^{-1}, \quad (17)$$
$$\hat{\boldsymbol{x}}_k^- = \boldsymbol{A}_l \hat{\boldsymbol{x}}_{k-1}^+ + \boldsymbol{B}_l \boldsymbol{u}_{k-1}, \quad (18)$$
$$\hat{\boldsymbol{x}}_k^+ = \hat{\boldsymbol{x}}_k^- + \boldsymbol{K}_k (y_k - \boldsymbol{C}_l \hat{\boldsymbol{x}}_k^-), \quad (19)$$
$$\boldsymbol{P}_k^+ = (\boldsymbol{I} - \boldsymbol{K}_k \boldsymbol{C}_l) \boldsymbol{P}_k^-, \quad (20)$$

where $\boldsymbol{P}_k^-$, $\boldsymbol{P}_k^+$, and $\boldsymbol{K}_k$ are the priori error covariance matrix at k, posteriori error covariance matrix at k, and the Kalman gain at k, respectively. The matrix $\boldsymbol{Q}_{kf,k-1}$ is the process noise covariance matrix and $\boldsymbol{R}_{kf,k}$ is the measurement noise covariance matrix.

3.3 Extended Kalman Filter (EKF) Estimator

Here, the system nonlinear model described in (14) is utilized. The Jacobian matrix of the state function $\boldsymbol{f}_{k-1}$ is computed with respect to the state vector $\boldsymbol{x}_{k-1}$,

$$\boldsymbol{F}_{k-1} = \frac{\partial \boldsymbol{f}_{k-1}}{\partial \boldsymbol{x}_{k-1}} = \begin{pmatrix} \frac{\partial f_{1,k-1}}{\partial x_{1,k-1}} & \frac{\partial f_{1,k-1}}{\partial x_{2,k-1}} & \frac{\partial f_{1,k-1}}{\partial \boldsymbol{x}_{3,k-1}} & \frac{\partial f_{1,k-1}}{\partial x_{4,k-1}} \\ \frac{\partial f_{2,k-1}}{\partial x_{1,k-1}} & \frac{\partial f_{2,k-1}}{\partial x_{2,k-1}} & \frac{\partial f_{2,k-1}}{\partial \boldsymbol{x}_{3,k-1}} & \frac{\partial f_{2,k-1}}{\partial x_{4,k-1}} \\ \frac{\partial \boldsymbol{f}_{3,k-1}}{\partial x_{1,k-1}} & \frac{\partial \boldsymbol{f}_{3,k-1}}{\partial x_{2,k-1}} & \frac{\partial \boldsymbol{f}_{3,k-1}}{\partial \boldsymbol{x}_{3,k-1}} & \frac{\partial \boldsymbol{f}_{3,k-1}}{\partial x_{4,k-1}} \\ \frac{\partial f_{4,k-1}}{\partial x_{1,k-1}} & \frac{\partial f_{4,k-1}}{\partial x_{2,k-1}} & \frac{\partial f_{4,k-1}}{\partial \boldsymbol{x}_{3,k-1}} & \frac{\partial f_{4,k-1}}{\partial x_{4,k-1}} \end{pmatrix}, \quad (21)$$

$$\frac{\partial f_{1,k-1}}{\partial x_{1,k-1}} = 1, \frac{\partial f_{1,k-1}}{\partial x_{2,k-1}} = T_s, \frac{\partial f_{1,k-1}}{\partial \boldsymbol{x}_{3,k-1}} = \boldsymbol{0}_{1\times 4},$$
$$\frac{\partial f_{1,k-1}}{\partial x_{4,k-1}} = 0, \frac{\partial f_{2,k-1}}{\partial x_{1,k-1}} = \frac{T_s(S_b + S_{rs})}{m + m_\infty},$$
$$\frac{\partial f_{2,k-1}}{\partial x_{2,k-1}} = 1 + \frac{T_s}{m + m_\infty}\big[- \rho A_w C_d (x_{2,k-1} - v_f) - \alpha F_n \mu_d \operatorname{sech}^2(\alpha x_{2,k-1}) - \mu_v - F_n(\mu_s - \mu_d)\alpha e^{-(\frac{|x_{2,k-1}|}{v_s})^2} \operatorname{sech}^2(\alpha x_{2,k-1}) - \frac{2F_n(\mu_s - \mu_d)x_{2,k-1}}{v_s^2} e^{-(\frac{|x_{2,k-1}|}{v_s})^2} \tanh(\alpha x_{2,k-1})\big],$$

$$\frac{\partial f_{2,k-1}}{\partial \boldsymbol{x}_{3,k-1}} = \frac{-T_s \boldsymbol{C}_r}{m + m_\infty}, \frac{\partial f_{2,k-1}}{\partial x_{4,k-1}} = \frac{T_s}{m + m_\infty}, \frac{\partial \boldsymbol{f}_{3,k-1}}{\partial x_{1,k-1}} = 0,$$
$$\frac{\partial \boldsymbol{f}_{3,k-1}}{\partial x_{2,k-1}} = T_s \boldsymbol{B}_r, \frac{\partial \boldsymbol{f}_{3,k-1}}{\partial \boldsymbol{x}_{3,k-1}} = \boldsymbol{I} + T_s \boldsymbol{A}_r, \frac{\partial \boldsymbol{f}_{3,k-1}}{\partial x_{4,k-1}} = 0,$$
$$\frac{\partial f_{4,k-1}}{\partial x_{1,k-1}} = \frac{\partial f_{4,k-1}}{\partial x_{2,k-1}} = 0, \frac{\partial f_{4,k-1}}{\partial \boldsymbol{x}_{3,k-1}} = \boldsymbol{0}_{1\times 4}, \frac{\partial f_{4,k-1}}{\partial x_{4,k-1}} = 1.$$

Similarly, the Jacobian matrices of the state function $\boldsymbol{f}_{k-1}$ with respect to the process noise vector $\boldsymbol{w}_{k-1}$, the measurement function $\boldsymbol{g}_k$ with respect to $\boldsymbol{x}_k$, and the measurement function $\boldsymbol{g}_k$ with respect to the measurement noise $\boldsymbol{\sigma}_k$, are evaluated as

$$\boldsymbol{W}_{k-1} = \frac{\partial \boldsymbol{f}_{k-1}}{\partial \boldsymbol{w}_{k-1}} = T_s \boldsymbol{I}_{7\times 7}.$$
$$\boldsymbol{H}_k = \frac{\partial \boldsymbol{g}_k}{\partial \boldsymbol{x}_k} = (1\ 0\ 0\ \boldsymbol{0}_{1\times 4}\ 0).$$
$$\boldsymbol{D}_k = \frac{\partial \boldsymbol{g}_k}{\partial \boldsymbol{\sigma}_k} = (1\ 0\ 0\ \boldsymbol{0}_{1\times 4}\ 0).$$

After initiating the posteriori state vector $\hat{\boldsymbol{x}}_{k-1}^+$, the posteriori estimation error covariance matrix $\boldsymbol{P}_{k-1}^+$ and evaluating the state Jacobian matrix $\boldsymbol{F}_{k-1}$ at the initial $\hat{\boldsymbol{x}}_{k-1}^+$, the extended Kalman filter estimate of the state vector is computed as follows

$$\boldsymbol{P}_k^- = \boldsymbol{F}_{k-1} \boldsymbol{P}_{k-1}^+ \boldsymbol{F}_{k-1}^\top + \boldsymbol{W}_{k-1} \boldsymbol{Q}_{ekf,k-1} \boldsymbol{W}_{k-1}^\top \quad (22)$$
$$\hat{\boldsymbol{x}}_k^- = \boldsymbol{f}_{k-1}(\hat{\boldsymbol{x}}_{k-1}^+, u_{k-1}, \boldsymbol{0}) \quad (23)$$
$$\boldsymbol{K}_k = \boldsymbol{P}_k^- \boldsymbol{H}_k^\top \big(\boldsymbol{H}_k \boldsymbol{P}_k^- \boldsymbol{H}_k^\top + \boldsymbol{D}_k \boldsymbol{R}_{ekf,k} \boldsymbol{D}_k^\top\big)^{-1} \quad (24)$$
$$\hat{\boldsymbol{x}}_k^+ = \hat{\boldsymbol{x}}_k^- + \boldsymbol{K}_k \big[y_k - \boldsymbol{g}_k(\hat{\boldsymbol{x}}_k^-, \boldsymbol{0})\big] \quad (25)$$
$$\boldsymbol{P}_k^+ = \big(\boldsymbol{I} - \boldsymbol{K}_k \boldsymbol{H}_k\big) \boldsymbol{P}_k^- \quad (26)$$

4. RESULTS AND DISCUSSIONS

The developed state estimators were examined at different testing scenarios — both in wave environment and electric loading conditions. The estimation goodness was evaluated using the normalized mean square error (NMSE), which measures the discrepancy between the true and estimated states. Here, the true excitation force $f_{ex,k}$ is the one actually experienced by the floater in the WEC plant and it is calculated using the LTI model described in (3). Another performance metric is the incident energy drop (IED), which is calculated as

$$IED = \frac{E_{inc} - \hat{E}_{inc}}{E_{inc}} \times 100, \quad (27)$$

where E_{inc} and $\hat{E}_{inc}$ are the true and estimated incident energy. The true incident energy is computed as $E_{inc} =$

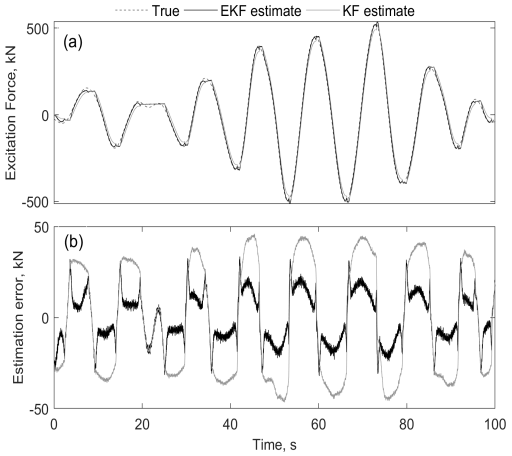

Fig. 3. The EKF and KF estimators performance in estimating $f_{ex,k}$ when $H_s = 3$ m and $T_p = 13$ s wave is applied under linear load.

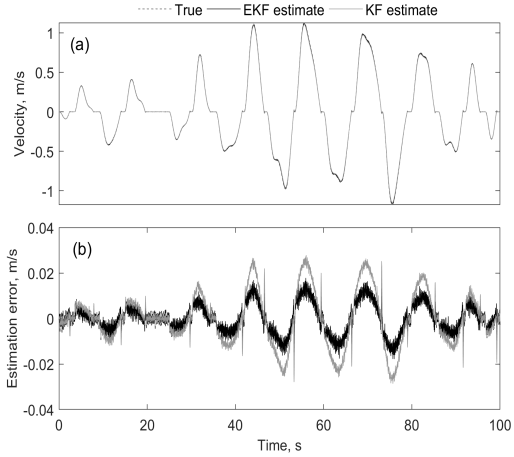

Fig. 4. The EKF and KF estimators performance in estimating v_k when $H_s = 3$ m and $T_p = 13$ s wave is applied under linear load.

$T_s \sum_{k=1}^{m} f_{ex,k} v_k$, whereas the estimated incident energy is $\hat{E}_{inc} = T_s \sum_{k=1}^{m} \hat{f}_{ex,k} \hat{v_k}$. The upper limit of the summation m is the simulation run time duration. The simulations were carried out in MATLAB/Simulink.

First, the estimation goodness was evaluated for both estimators when a sea-state of significant height $H_s = 3$ m and peak period $T_p = 13$ s is applied. The terminals of the PMLG was connected to a linear three phase resistive load with per-phase resistance of 40 Ω. Both the drag force and the friction force were applied on the WEC system plant. As shown in Fig. 3, both estimators performed well in estimating the true excitation force and heave velocity signals. The NMSE of the estimated excitation force $\hat{f}_{ex,k}$ for the EKF estimator is approximately 93.91%, while the KF estimator produced an NMSE score of 86.01%. As for the heave velocity estimate, the EKF estimator managed to produce a very accurate estimate with NMSE of 98.67%, whereas the KF performed as well with NMSE of 97.52% as shown in Fig. 4. Using the EKF estimates, the accumulated incident energy drop (IED) was around 24.68%, meanwhile, the KF estimater performed poorly in this regard with an IED of 69.68%. Next, the friction force was omitted and the performance of the estimators was noted (Fig. 5). As expected, both estimators produced better $f_{ex,k}$ estimates, with NMSE scores of 96.93% and 94.38% for the EKF and KF estimators, respectively. This is due to the absence of the highly nonlinear friction force in the WEC plant. An improvement was also recorded in regard to the IED metric, with 9.97% and 51.48% for EKF and KF estimators, respectively. It is noteworthy to mention that despite the fact that both estimators produced fairly good estimates "statistically", that did not guarantee good energy capturing performance, knowing that the WEC control strategy will be largely dictated by the estimated excitation force $\hat{f}_{ex,}$. A more rapid sea state ($H_s = 2.75$ m and $T_p = 7$ s) was applied to investigate the effect of changing the wave frequency on the estimators performance under a linear (resistive) load. As shown in Fig. 6, the EKF estimator performed generally well, though the NMSE score (i.e., 87.88%) for $f_{ex,k}$ is slightly lower than that of the slower sea state (i.e., $T_p = 13$ s) discussed earlier. Meanwhile, the KF

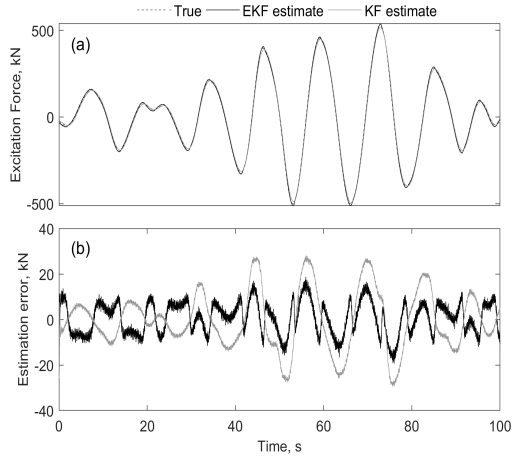

Fig. 5. The EKF and KF estimators performance in estimating $f_{ex,k}$ when $H_s = 3$ m and $T_p = 13$ s wave is applied under linear load, while neglecting the friction force.

estimator suffered from a great drop in the estimation NMSE (i.e., 69.34%). Despite the accuracy deterioration, both estimators suffered from lower IED, that is 18.59% and 63.10% for EKF and KF estimators, respectively.

Finally, the proposed EKF estimator was tested under different electrical loading conditions. Instead of a linear resistive load, a nonlinear load was utilized. As shown in Fig. 1, the PMLG is connected to a three phase diode rectifier. The output of the rectifier is connected to a smoothing capacitor and a 40 Ω load resistor. This nonlinear loading circuit offers a challenging scenario for testing the estimator due to the discontinuities and harmonics present in the stator current and therefore in the input damping electromagnetic force $f_{em,k}$. As shown in Fig. 7(a), the EKF estimator did not experience any noticeable deterioration in performance in regard to NMSE, where the EKF estimator scored 88.73% when nonlinear load was applied, contrary to 87.88% in case of linear load. However, the EKF estimator scored a significantly better IED score (8.68%) under nonlinear loading than linear loading (18.59%). This can be explained that under the nonlinear loading, the damping PTO force $f_{em,k}$ is much larger than

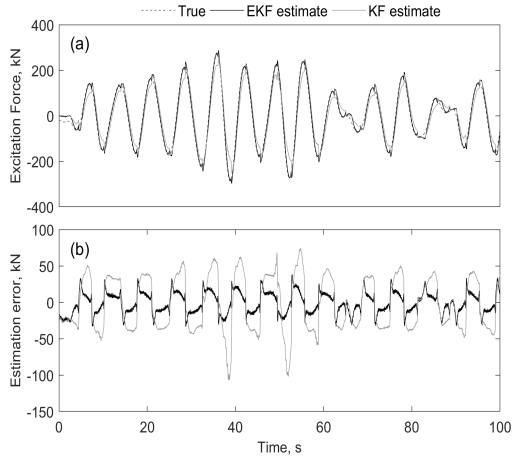

Fig. 6. The EKF and KF estimators performance in estimating $f_{ex,k}$ when $H_s = 2.75$ m and $T_p = 7$ s wave is applied under linear load.

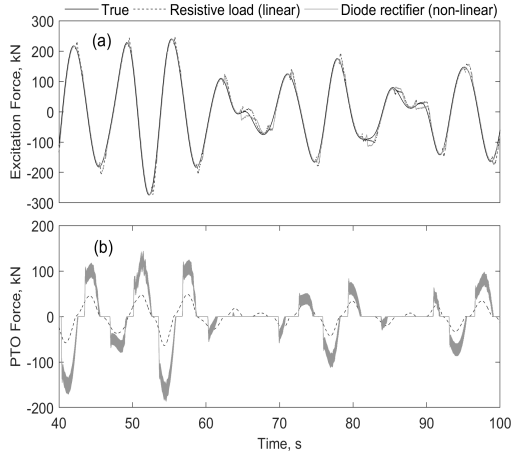

Fig. 7. The EKF estimator performance under two different loading conditions when a $H_s = 2.75$ m and $T_p = 7$ s wave is applied.

that of a linear loading as shown in Fig. 7(b). This results in lower heave velocities, which in turn minimizes the effect of the velocity dependent nonlinear dynamics (e.g., drag and friction forces).

5. CONCLUSION

In this work, a state estimator based on an extended Kalman filter for estimating the crucial wave excitation force and heave velocity in real-time is proposed. The estimator is based on a comprehensive nonlinear model that characterizes the wave-floater-PTO dynamic interactions. The estimator was assessed rigorously under various modeling, sea-state environment, and electric loading conditions. In all the testing scenarios, the EKF estimator managed to produce accurate estimates with NMSE scores not less than 85%.

REFERENCES

Abdelkhalik, O., Zou, S., Robinett, R., Bacelli, G., and Wilson, D. (2016). Estimation of excitation forces for wave energy converters control using pressure measurements. *Int. J. Control*, 90, 1793–1805.

Babarit, A. and Clement, A. (2006). Optimal latching control of a wave energy device in regular and irregular waves. *Applied Ocean Research*, 28, 77–91.

Brown, P. and McPhee, J. (2016). A continuous velocity-based friction model for dynamics and control with physically meaningful parameters. *Journal of Computational and Nonlinear Dynamics*, 11, 054502–054502.

Falnes, J. (2002). *Ocean Waves and Oscillating Systems*. Cambridge University Press.

Jama, M. and Wahyudie, A. (2017). Online damping strategy for controlling heaving wave energy converters using three-phase bridge boost rectifier. *IEEE Access*, 5, 7682–7691.

Jama, M., Wahyudie, A., and Noura, H. (2018). Robust predictive control for heaving wave energy converters. *Control Engineering Practice*, 77, 138–149.

Kracht, P., Perez-Becker, S., Richard, J.B., and Fischer, B. (2013). Two-dimensional nonlinear analysis of an untethered spherical buoy due to wave loading. *Journal of Computational and Nonlinear Dynamics*, 8, 041019(1)–041019(12).

Kracht, P., Perez-Becker, S., Richard, J.B., and Fischer, B. (2015). Performance improvement of a point absorber wave energy converter by application of an observer-based control: Results from wave tank testing. *IEEE Trans. Ind. Appl.*, 51, 3426–3434.

Nguyen, H. and Tona, P. (2017). Wave excitation force estimation for wave energy converters of the point-absorber type. *IEEE Trans on Control System Technology*, 26, 2173–2181.

Taghipoura, R., Pereza, T., and Moan, T. (2008). Hybrid frequency-time domain models for dynamic response analysis of marine structures. *Ocean Engineering*, 35, 685—-705.

Appendix A. DESIGN PARAMETERS

A.1 WEC paramters

The following are the values of the different WEC design parameters:
$m = 30189$ kg, $\rho = 1025$ kg/m^3, $A_w = 19.64$ m^2, $m_\infty = 28518$ kg, $S_b = 197370$ N/m, $S_{rs} = 60000$ N/m, $C_d = 1$, $F_n = 12000$ N, $\mu_d = 1$, $\mu_v = 2$, $\mu_s = 2$, $v_s = 1$ m/s, $\alpha = 10$.

$$\boldsymbol{A}_r = \begin{bmatrix} -3.2914 & -7.9461 & -7.7067 & -4.2272 \\ 1 & 0 & 0 & 0 \\ 0 & 1 & 0 & 0 \\ 0 & 0 & 0 & 1 \end{bmatrix}, \boldsymbol{B}_r = \begin{bmatrix} 1 \\ 0 \\ 0 \\ 0 \end{bmatrix},$$

$\boldsymbol{C}_r = [14745\ 52918\ 41145\ 0]$.

A.2 State estimators parameters

$Q_{kf} = q'_{kf} q_{kf}$,
$q_{kf} = [1\times10^{-5}, 1\times10^{-5}, 1\times10^{-15}, 1\times10^{-15}, 1\times10^{-15}, 1\times10^{-15}, 5\times10^{5}]$,
$R_{kf} = 200$,
$Q_{ekf} = q'_{ekf} q_{ekf}$,
$q_{ekf} = [1\times10^{-5}, 1\times10^{-5}, 1\times10^{-15}, 1\times10^{-15}, 1\times10^{-15}, 1\times10^{-15}, 1\times10^{10}]$,
$R_{ekf} = diag(100, 1\times10^{-10}, 1\times10^{-10}, 1\times10^{-10}, 1\times10^{-10}, 1\times10^{-10}, 1\times10^{-10})$.